Atmos. Chem. Phys. Discuss., 13, 28695–28727, 2013
www.atmos-chem-phys-discuss.net/13/28695/2013/
doi:10.5194/acpd-13-28695-2013

Atmospheric Chemistry and Physics Discussions

Estimating the volcanic emission rate and atmospheric lifetime of SO_2 from space: a case study for Kīlauea volcano, Hawai'i

S. Beirle[1], C. Hörmann[1,2], M. Penning de Vries[1], S. Dörner[1], C. Kern[3], and T. Wagner[1]

[1]Max-Planck-Institut für Chemie, Mainz, Germany
[2]Institut für Umweltphysik, Universität Heidelberg, Heidelberg, Germany
[3]USGS Cascades Volcano Observatory, Vancouver, Washington, USA

Received: 20 September 2013 – Accepted: 25 October 2013 – Published: 4 November 2013

Correspondence to: S. Beirle (steffen.beirle@mpic.de)

Published by Copernicus Publications on behalf of the European Geosciences Union.

Abstract

We present an analysis of SO_2 column densities derived from GOME-2 satellite measurements for the Kīlauea volcano (Hawai'i) for 2007–2012. During a period of enhanced degassing activity in March–November 2008, monthly mean SO_2 emission rates and effective SO_2 lifetimes are determined simultaneously from the observed downwind plume evolution and ECMWF wind fields, without further model input. Kīlauea is particularly suited for quantitative investigations from satellite observations owing to the absence of interfering sources, the clearly defined downwind plumes caused by steady trade winds, and generally low cloud fractions. For March–November 2008, the effective SO_2 lifetime is 1–2 days, and Kīlauea SO_2 emission rates are 9–21 kt day^{-1}, which is about 3 times higher than initially reported from ground-based monitoring systems.

1 Introduction

Sulphur dioxide (SO_2) plays an important role in atmospheric chemistry. It directly affects air quality as it is a respiratory irritant, and it is one of the main causes of acid rain. Beyond this, atmospheric SO_2 is also highly relevant for the Earth's climate, as it is an important precursor of aerosols, which affect the planet's radiative budget both directly and indirectly (e.g. by influencing the number and size of cloud droplets).

SO_2 is removed from the atmosphere by dry and wet deposition (in the boundary layer), or by chemical conversion to sulphuric acid (H_2SO_4). In the gas phase, this conversion is initiated by the OH radical. The respective SO_2 lifetime in the troposphere is about two weeks (von Glasow et al., 2009). However, heterogeneous reactions on cloud droplets convert SO_2 into H_2SO_4 on much shorter time-scales of days or even hours (von Glasow et al., 2009).

Volcanoes are a large natural source of SO_2 with high temporal and spatial fluctuations, and total emissions are still highly uncertain. Kīlauea volcano, located on

ACPD
13, 28695–28727, 2013

Hawai'i Island, has shown persistent effusive SO_2 degassing for over more than 3 decades. A period of particularly high gas emissions began in early 2008 with the lead up and opening of a new vent within the Halema'uma'u summit crater. A detailed overview about the dates, locations, specification of volcanic activity, and ground-based SO_2 emission rate estimates is provided by Elias and Sutton (2012).

Its location in the remote Pacific, far from other SO_2 sources, along with relatively steady northeasterly trade winds make Kīlauea a "natural laboratory" (Yuan et al., 2011), well suited e.g. for the investigation of aerosol indirect effects from satellite observations (Yuan et al., 2011; Eguchi et al., 2011).

During recent decades, methods for the quantification of volcanic SO_2 emissions from spectroscopic measurements have been developed and refined (e.g., Moffat and Millan, 1971; Galle et al., 2002; Mori and Burton, 2006). In addition to such ground-based measurements, satellite measurements of atmospheric trace gases (Burrows et al., 1999) have revolutionized our knowledge of abundance, sources and transport of various pollutants over the last decades (e.g., Monks and Beirle, 2011, and references therein). They provide new potential for monitoring volcanic activity, and have been applied to estimate burdens and fluxes of SO_2 (e.g., Khokhar et al., 2005; Carn et al., 2005, 2008; Krotkov et al., 2010).

Recently, it has been demonstrated that lifetimes of trace gases can also be quantified by analysing the downwind decay of point source emissions as observed from satellites, see e.g. Leue et al. (2001) and Beirle et al. (2004, 2011) for Nitrogen oxides or Krotkov et al. (2010) for SO_2.

In this study we present an analysis of the downwind evolution of the SO_2 plume from Kīlauea, as derived from GOME-2. By combining the satellite measurements with ECMWF wind fields, we demonstrate that an effective SO_2 lifetime can be determined from a relatively simple and robust mathematical analysis. In addition, the SO_2 emission rate from Kīlauea is quantified and compared to ground-based estimates.

ACPD
13, 28695–28727, 2013

2 Method

2.1 SO_2 from GOME-2

GOME-2, the second Global Ozone Monitoring Experiment (Callies et al., 2000) was launched in October 2006 on board the MetOp-A satellite. It is operated in a sun-synchronous orbit, crossing the equator at about 9:30 LT. Nominal ground pixel size is 80 km × 40 km, and global coverage is attained every 1.5 days.

SO_2 Slant Column Densities (SCDs), i.e. concentrations integrated along the mean light path, are derived from spectral GOME-2 measurements in the UV by Differential Optical Absorption Spectroscopy (DOAS) (Platt and Stutz, 2008), as described in Hörmann et al. (2013). SCDs are converted into Vertical Column Densities (VCDs), i.e. vertically integrated concentrations, via the so-called air mass factor (AMF). AMFs are calculated using the Monte-Carlo radiative transfer model (RTM) McArtim (Deutschmann et al., 2011) for cloud free conditions and different a priori aerosol scenarios (see Sect. 2.2). The plume altitude for both SO_2 and aerosols was set to 1.5–2.5 km (see Sect. 2.3).

The SO_2 detection limit for the SCDs of individual ground pixels has increased from about 1×10^{16} molec cm^{-2} in 2007 to about 2×10^{16} molec cm^{-2} in 2011 due to instrument degradation (Hörmann et al., 2013). For the given AMFs, this corresponds to a VCD detection limit of 1.3–2.7 $\times 10^{16}$ molec cm^{-2}, or 0.5 to 1 Dobson Units (DU).

The individual satellite observations are gridded on a regular lat/lon grid with 0.1° resolution. Only ground pixels with an effective cloud fraction below 20 % are considered, using the GOME-2 cloud product based on the FRESCO algorithm (Wang et al., 2008). Figure 1 shows the gridded monthly mean SO_2 VCDs for 2007–2012. Enhanced SO_2 column densities can be observed southwest of Hawai'i Island during several months, especially in 2008. For August 2008, a zoomed map is shown in Fig. 2, providing additional information on the location of Kīlauea on Hawai'i, elevation contour lines, and mean wind directions for different altitude levels.

ACPD
13, 28695–28727, 2013

2.2 Aerosol and cloud effects

Satellite measurements are affected by aerosols and clouds due to their influence on radiative transfer. Aerosols and clouds generally shield the troposphere below, but increase the satellite's sensitivity for trace gases within or above the aerosol/cloud layer due to multiple scattering and the increased albedo. Here we describe the detailed treatment of aerosols and clouds specified for the conditions at Kīlauea.

Aerosols are formed within the volcanic plume by conversion of SO_2 in H_2SO_4 and subsequent formation of, or uptake in, aqueous droplets. Thus, we assume the same vertical profile for SO_2 and aerosols. During the volcano's active phase in 2008, the aerosol optical depth (AOD) was significantly enhanced above background in the plume region over ocean, reaching monthly mean values of 0.35 (compare Beirle et al., 2012) as measured by MODIS TERRA (at 550 nm).

In order to correct for the influence of plume aerosols on radiative transfer, three sets of VCDs are calculated for a priori AOD of 0, 0.4, and 1 (at 315 nm), respectively. The AMFs increase linearly by about 20 % for an increase of AOD from 0 to 1. For the calculation of the actual monthly mean SO_2 VCD, these a priori VCDs are interpolated according to the "real" AOD. The latter is taken from the monthly mean MODIS TERRA AOD (with a local overpass time similar to that of GOME-2), multiplied by 2 (corresponding to an Ångstrom coefficient of 1.24) to account for the AOD wavelength dependency. We estimate the remaining uncertainty due to aerosol effects to be negligible (< 10 %).

To minimize cloud effects, only observations with cloud fractions below 20 % are considered. The remaining cloud effects could in principle be corrected by radiative transfer calculations, as long as the vertical profiles of both SO_2 and clouds are accurately known. However, this is not the case: the SO_2 plume altitude has some uncertainty (see Sect. 2.3), and the cloud altitudes derived from satellite observations have high uncertainties for low cloud fractions. Thus, we decided to consider the observations with cloud fractions below 20 % as "cloud free", without further corrections. We justify

ACPD
13, 28695–28727, 2013

this by performing our analysis for different a priori thresholds for the effective cloud fraction. The dependency of the resulting VCDs on the cloud fraction threshold turned out to be negligibly small (see Sect. 4). This indicates that the remaining cloud effects (shielding vs. multiple scattering/albedo increase) at least partly cancel out.

2.3 Plume altitude

The SO_2 plume altitude has a large impact on our analysis via two different effects. First, the sensitivity of the satellite measurements depends on the trace gas vertical profile. The sensitivity generally decreases towards the ground for low albedo such as over ocean. Second, the horizontal wind speed, needed for the lifetime estimate as explained below, depends on altitude as well. Thus, for the emission rate estimate, an accurate a priori plume altitude is needed.

Here we define upper and lower thresholds for the SO_2 plume altitude by the following considerations:

- The monthly mean maps for March–November 2008 reveal a clear SO_2 outflow with a well-defined direction. We determine the mean plume direction as the slope of a weighted linear fit applied to the lat/lon coordinates of all grid pixels with a VCD above 3×10^{16} molec cm^{-2}. For August, the resulting plume direction is displayed as grey arrow in Fig. 2. By comparison to ECMWF wind vectors at different altitudes, shown in shades of green, an upper bound of the SO_2 plume altitude can be derived. In particular, the August plume is clearly below 3 km, as the plume direction reveals a small southward component (consistent with ECMWF winds below 2.5 km), while ECMWF wind fields above 2.5 km show a northward component instead. For May–November 2008, ECMWF winds at 1.5–2.5 km reveal the best agreement to the observed plume direction (Fig. 3).

- Kīlauea's summit vent is located at about 1.1 km a.s.l. Although this altitude is generally within the maritime boundary layer (MBL) around Hawai'i of approximately 2 km (Cao et al., 2007), the plume from the summit is generally buoyant enough

ACPD
13, 28695–28727, 2013

to stay at the upper edge of the MBL or even break through the inversion at times (Elias and Sutton, 2012). Emissions from the East Rift, on the other hand, are emitted at only 0.7 km altitude and tend to be less buoyant, thus typically staying in the mid MBL (A. J. Sutton, personal communication, 2013). Therefore, the satellite will be less sensitive to these emissions than those originating from the summit vent.

After taking the above considerations into account, we estimate that an effective plume altitude of between 1.5 and 2.5 km most accurately describes the plume's location in 2008. This altitude range yields the best agreement between ECMWF wind direction and plume direction for March–November (see Fig. 3), is in good agreement with the altitude range given by Elias and Sutton (2012), and is consistent with the altitude of the aerosol plume derived by Eguchi et al. (2011) based on CALIOP measurements.

For the conversion of SCDs into VCDs, we thus calculate AMFs for a priori box profiles from 1.5 and 2.5 km altitude for both SO_2 and aerosols.

2.4 Downwind plume evolution

We investigate the downwind evolution of SO_2 from Kīlauea based on monthly mean VCD maps. Due to the stable meteorological conditions, i.e. steady trade winds, the outflow is headed westwards. Therefore, we estimate the background SO_2 VCD from upwind measurements east of Hawai'i (at 150–153° W). The background-corrected monthly mean SO_2 VCDs are then integrated in latitudinal direction (10–25° N), resulting in "line densities" (LD) as a function of longitude (the small southward component is eliminated by the latitudinal integration). By finally multiplying the LDs with the longitudinal wind speed u from ECMWF averaged over 1.5–2.5 km altitude, a longitudinal SO_2 flux is derived as a function of time t since emission from the volcano. Figure 4 displays the observed SO_2 flux for March–November 2008 in red.

ACPD
13, 28695–28727, 2013

2.5 Lifetime and emission fit procedure

SO_2 lifetime and emission rates are derived simultaneously by fitting the model function $F(t)$ to the observed SO_2 flux with a non-linear least squares algorithm:

$$F(t) = E \times e^{-t/\tau}, \quad (1)$$

with the emission rate E and the lifetime τ as fit parameters. In addition, $F(t)$ is smoothed by a Gaussian with a standard deviation of $\sigma_t = \sigma_x/u$, where u is the monthly mean wind speed in the plume, and σ_x is 80 km in order to account for the GOME-2 across-track ground pixel size.

A very similar approach was used by Beirle et al. (2011) to estimate NO_x lifetimes and emissions from megacities. In the case of SO_2 from Kīlauea, however, some simplifications/modifications were possible/necessary:

- As the lifetime of SO_2 is considerably longer than that of NO_x, the considered spatial/temporal scales are much larger (≈ thousand km/hundred h).
- Due to the steady trade winds, at least during summer, a sorting of the observations by wind direction is not necessary here.
- As wind direction is stable and there are no interfering sources of SO_2, the background VCD can directly be estimated from upwind measurements, while it had to be included as free fit parameter in Beirle et al. (2011).
- In Beirle et al. (2011), an e-folding distance x_0 is fitted to the line densities as function of x, and the lifetime is then derived from x_0 by division by the mean wind speed. In the current study, the wind speed can change significantly with distance from the volcano (as larger distances have to be considered). Thus, the downwind flux is first transferred into a function of time by variable transformation via the local wind speeds ($t = x/u$). The subsequent fit directly yields the effective lifetime τ.

ACPD
13, 28695–28727, 2013

Note that the downwind reduction of the SO_2 flux with time shown in Fig. 4 in fact reflects the chemical conversion or depletion of SO_2, and is not caused by dilution of the plume, as the concentrations are integrated vertically (by the column measurement) and latitudinally (10–25° N). The outflow out of this area can be neglected, as can easily be checked by extending the latitude range over which integration occurs. This had only a small impact on the results (see Sect. 4.1 and Table 1).

The simultaneous fit of SO_2 lifetime and emission rate as described above requires a well defined SO_2 plume and steady easterly winds. Thus, we apply it for the months March–November 2008 with the highest observed SO_2 VCDs far above the detection limit. During this period, the mean *u*-component of ECMWF wind is negative (easterly) for all 6 hourly time-steps, except for April (8 time-steps with westerly wind) and October (1 time-step with westerly wind). Consequently, the background estimated east from Hawai'i is biased high, resulting in negative VCDs and fluxes for those months (compare Fig. 4).

In addition to the fitted SO_2 lifetime and emission rates for this particular period, we also provide a rough emission rate estimate based on the monthly mean VCDs for the complete time series 2007–2012 (see Sect. 3).

3 Results

Figure 4 displays the observed (red) and fitted (black) downwind evolution of the longitudinal SO_2 flux. Despite the fact that the processes responsible for SO_2 removal from the atmosphere, i.e. gas-phase reactions with OH and heterogeneous reactions on cloud droplets, have significantly different time constants, the observed downwind loss of SO_2 can be described by a single first-order time constant. Figure 5 shows the resulting monthly mean SO_2 lifetimes and emission rates.

The derived SO_2 lifetimes range from 16–57 h. They show a seasonal cycle and are anti-correlated to the monthly mean cloud fraction: lifetimes are highest in summer when cloud cover is smallest, and shorter for higher cloud fractions in spring and

ACPD
13, 28695–28727, 2013

autumn. This anti-correlation is in accordance to the impact of heterogeneous reactions on cloud droplets. On average, we find a mean SO_2 lifetime of 1.56 days, which is consistent with previous studies. For instance, Lelieveld et al. (1997) give an average SO_2 lifetime of 2 days, based on the general circulation model ECHAM. Lee et al. (2011) derived mean lifetimes of 19 ± 7 h from in-situ measurements over the Eastern US in summer.

Our derived SO_2 lifetimes are significantly longer than the 6 h (half-life) estimated by Porter et al. (2002) for the East Rift plume for one day of measurements. However, our values are arguably more robust because SO_2 is measured directly instead of indirectly deriving an aerosol mass from an AOD, the plume is measured for hundreds of km after emission into the atmosphere instead of only the first 9 km, and the actual evolution of SO_2 column densities is quantified over time as opposed to simply taking a single snapshot. Nevertheless, it is also possible that heterogeneous reactions on volcanic aerosols reduce the SO_2 lifetime for the first few minutes after emission (see Sect. 4.2).

The fitted monthly mean SO_2 emission rates range from 9 to 21 kt day^{-1}. Integrated emissions from March to October 2008 are 3.5 Tg (with an uncertainty of about 50 %, see Sect. 4), which is higher, but of the same order of magnitude as the estimate of 1.8 ± 1.2 Tg given by Eguchi et al. (2011), based on a comparison of SCIAMACHY observations to model simulations.

Figure 6 displays the derived emission rates in comparison to the monthly mean SO_2 VCD downwind of the volcano. A clear correlation can be seen ($R = 0.92$). By assuming that the fitted linear relation between emission rates and spatio-temporal mean column densities also holds for other months with lower SO_2 column densities, emission rates can be estimated for the complete timeseries 2007–2012 (see Fig. 7, where emission rates reported by Elias and Sutton (2012) are shown for comparison, see Sect. 4.3).

Note that this assumption of a linear relation between emission rates and mean column densities implies that the SO_2 AMFs and lifetime do not change with time.

ACPD
13, 28695–28727, 2013

While the fitted slope in Fig. 6 corresponds to an effective SO_2 lifetime of 2 days, which is in good agreement with the lifetimes obtained from the plume evolution during the individual months, the assumption of a constant AMF can only be considered a rough estimate. In the 2007–2010 time period, the ratio of emission rates from the summit and from Pu'u 'Ō'ō varied with the opening of the summit Overlook Vent and episodic unrest related to the ongoing East Rift eruption (Elias and Sutton, 2012). Due to the different emission altitudes of these two sources (which cannot be differentiated at the spatial resolution of the GOME-2 measurements), this variability is expected to influence the effective plume altitude, thereby modulating the AMF. This effect is particularly apparent in the data collected prior to the 2008 summit vent opening, as is discussed in Sect. 4.3.

4 Discussion

4.1 Uncertainties

Emission rates and lifetimes of SO_2 are derived from monthly mean GOME-2 measurements, involving cloud masking, spatial integration, and the fitting of a simple model function. The fit provides confidence intervals for τ and E, which are in the range of 15–30 % and 10–20 %, respectively. For April, the fit uncertainty is higher (60 % and 45 %), as the downwind SO_2 VCD becomes smaller than the upwind values, which can not be reproduced by the model function $F(t)$, and is caused by some days with westerly winds, affecting the background value at 150–153° W.

Additional uncertainties may arise due to the a priori settings. Table 1 lists the baseline settings made in our analysis, and compares the resulting mean emission rates and lifetimes for March–November 2008 to the respective results for various alternative a priori settings.

(a) We calculate monthly mean SO_2 VCDs for observations with cloud fractions below 20 %. Alternatively, we repeated our analysis for a lower or higher cloud fraction threshold. This variation of the cloud fraction threshold only has a minor impact on

ACPD
13, 28695–28727, 2013

the estimated lifetime, and hardly any effect on the emission rate. Thus, the actual choice of the cloud fraction threshold is not critical, and cloud effects on AMFs are negligible (at least up to a cloud fraction threshold of 30 %). This might be explained by clouds having a similar altitude as the SO_2 plume, where effects of shielding and multiple scattering/albedo increase on AMFs cancel out (compare Sect. 2.2).

(b) The SO_2 VCDs are integrated in latitudinal direction from 10–25° N in order to determine LDs. If a smaller integration interval (15–20° N) is chosen instead, this interval no longer covers the entire SO_2 plume, especially for larger distances from the vent. Consequently, the fitted lifetime is biased low (−17 %), as the lack of plume coverage in the downwind regions acts as an additional virtual sink. On the other hand, an increase of the latitude range over which integration takes place does not significantly change the derived SO_2 lifetime. Hence, the chosen range is appropriate, and the fitted lifetime represents chemical loss rather than dilution effects, as the full plume is covered.

(c) We fit τ and E over a time interval from −20 to 100 h, i.e. the range shown in Fig. 4. Variations of the time interval, i.e. choosing a longer or shorter time interval, have hardly any effect on the mean fit results. We also tested a time interval starting at 20 h, in order to avoid inhomogeneities due to terrain effects (ground albedo, wind speeds) over Island of Hawai'i. Even though the largest SO_2 fluxes are skipped for this fit interval, the fit results hardly changed.

(d) The treatment of the SO_2 background is also not critical. In the baseline algorithm, an a priori background correction is applied based on upwind measurements at 150–153° W. If, instead, B is added as a free fitting parameter in Eq. (1), as in Beirle et al. (2011), both E and τ change by only 5 %.

(e) The plume altitude has a strong impact on the resulting emission rates and lifetimes; a relatively small shift of the a priori plume altitude of ±0.5 km down or up

ACPD
13, 28695–28727, 2013

changes the total emissions by ≈ ±30 %. This is due to the altitude dependency of both, the instrument's sensitivity (affecting the VCD and thereby directly the fitted emission rates), and the horizontal wind speeds (affecting the conversion of line densities to fluxes, and thereby the fitted lifetime and emission rates). For the Kīlauea case study, both effects have the same sign (lower a priori plume altitude leads to higher emission rate estimates) and amplify instead of cancel each other. Note that the strong effect of the a priori plume altitude is also the main reason for the different results of this study compared to those reported previously at the ESA ATMOS conference (Beirle et al., 2012), which were based on a mean plume altitude of 2.5 km.

As argued in Sect. 2.3, we can constrain the mean plume altitude by comparison of the plume direction with the wind direction at different altitudes. In addition, CALIOP provides measurements of aerosols in the volcanic plume that are in good agreement with this altitude range. For individual months the a priori plume altitude of 1.5–2.5 km might be off (e.g. for March 2008, compare Fig. 3), but due to the consistency of height information deduced from different and independent datasets, we conclude that it represents the average plume altitude for the period of high SO_2 VCDs in 2008 well, with an uncertainty of about 0.5 km (on average).

Nevertheless, the strong effect of the a priori plume altitude makes it the dominating source of uncertainty for the derived emission rates.

Overall, we estimate the uncertainty of both fitted emission rates and effective lifetimes to be about 50 % for the mean of March–November 2008. For individual months, uncertainties might be higher, in particular for emission rates.

4.2 Temporal variability and non-linear effects

The fitted model function assumes one value for both E and τ. In reality, however, emissions as well as instantaneous lifetimes are highly variable:

ACPD
13, 28695–28727, 2013

– Volcanic emission rates can show high temporal fluctuations. This could lead to sampling artifacts due to the limited temporal coverage of the satellite observations. In the monthly mean, however, such effects at least partly cancel out, and the fitted emission rates actually represent the mean $\langle\rangle$ of the time-dependent emission rates E_i, as the mean of exponential decays of varying emission rates equals the exponential decay of the respective mean emission rate $\overline{E}$:

$$\left\langle E_i \exp\left(-\frac{t}{\tau}\right)\right\rangle = \langle E_i\rangle \exp\left(-\frac{t}{\tau}\right) = \overline{E}\exp\left(-\frac{t}{\tau}\right).$$

– For variations of the lifetime of SO_2, which are intrinsic due to the different removal processes, the situation is different insofar as τ in Eq. (1) is an argument of a non-linear function. Thus, the mean of different functions $\exp\left(-\frac{t}{\tau_i}\right)$ can not, in a strict mathematical sense, be transformed into a single function $\exp\left(-\frac{t}{\tau_{\text{eff}}}\right)$. Nevertheless, as shown in Fig. 4, the observed downwind plumes are well described by a single, effective time constant.

In order to investigate the effect of temporal variations of E and τ and the non-linearity in τ, we calculated synthetic downwind decays $F_i = E_i \exp\left(-\frac{t}{\tau_i}\right)$ for E_i being a normally distributed random number with $\sigma_E = \overline{E}/2$, and $\tau_{i,j}$ being a random number uniformly distributed between 1 and 60 h. The additional index j indicates that for each i, τ is assigned a new random number after a time step of length T. We calculated 10 000 individual downwind plumes (in a Lagrangian framework), and performed the fit of E and τ to the average downwind plume. Figure 8 and Table 2 summarise the results:

For high values of T (i.e., each decay has only one instantaneous lifetime), the fitted lifetimes match the mean of a priori lifetimes. However, for this scenario, the simulated downwind decay does not perfectly match the model function of a single time constant

ACPD
13, 28695–28727, 2013

as a consequence of the non-linearities discussed above. In addition, if the instantaneous rate constants $k_i = 1/\tau_i$ are averaged instead of the lifetimes, they deviate from the mean a priori k by 30 %.

For short values of T, on the other hand, the fit works well; the switch of time constants in the simulation results in a decay pattern which can well be described by a single time constant. The lifetime returned by the fit is significantly shorter than the mean of the lifetimes used for the simulations, while the respective average of rate constants matches the actual mean within 1 %. As the fitted emissions are in very good agreement with the a priori (±4 %), we conclude that the lifetime found by the fit, though different from the mathematical mean, is the appropriate quantity to link the mean SO_2 VCDs to the respective emission rates by mass balance ($E = \int(\mathrm{VCD})/\tau$), and, in this sense, represents the effective lifetime.

The situation may be different if variations of instantaneous lifetimes are not purely random, but systematic. For instance, if instantaneous lifetimes were always short close to the vent, e.g. due to heterogeneous reactions within the plume, a considerable fraction of SO_2 might be lost before it could be detected from space. For such a scenario, the initial emission rates might be considerably higher than those deduced from space.

4.3 Comparison to results from ground-based monitoring

The US Geological Survey (USGS) has been monitoring SO_2 emission rates from Kīlauea for several decades. Elias and Sutton (2012) report emission rates for 2007–2010 derived from stationary as well as vehicle-based spectroscopic measurements with the FLYSPEC system (Horton et al., 2006) downwind of the Kīlauea summit and East Rift (about 2–4 measurements per week). For retrieval details see Elias and Sutton (2012) and references therein. We compare the monthly mean emissions derived from GOME-2 data to the time series provided in Figs. 29 and 30 in Elias and Sutton (2012). Note that the summit emission values published in Elias and Sutton (2012), which are susceptible to underestimation owing to radiative transfer assumptions, have not yet been corrected for non-linear effects (see below).

ACPD
13, 28695–28727, 2013

Overall, our emission rate estimates based on GOME-2 are far higher than those reported in Elias and Sutton (2012). For total Kīlauea emissions in 2008, we find 3.9 Tg, in comparison to the 1.1 Tg in Elias and Sutton (2012) (Fig. 29 therein).

Recently, Kern et al. (2012) investigated the UV radiative transfer (RT) in volcanic plumes in detail and showed that SO_2 emissions obtained from spectroscopic measurements and DOAS-type analysis can be strongly biased for plumes that have large SO_2 column abundance or are optically dense. For a sample day (1 March 2010), a revised analysis, accounting for RT and non-linearities due to strong SO_2 absorption, results in a doubling of the emission rates compared to the FLYSPEC standard evaluation (Kern et al., 2012). Note that generally satellite measurements can be affected by non-linearities as well (Hörmann et al., 2013). Due to the large ground pixels and the view from above, however, the effects are by far smaller than for slant observations from the ground in very close proximity to the source.

The findings of Kern et al. (2012) are discussed in Elias and Sutton (2012), and a first, preliminary analysis accounting for these effects is presented. For this revised analysis, higher emission rates are derived (1.5 Tg instead of 1.1 Tg for 2008), but are still significantly lower than those derived from GOME-2 in this study. In order to understand these discrepancies, further detailed investigation is necessary.

Given the added complexity of retrieving accurate SO_2 emission rates when extremely high column densities are encountered, and given that the ground-based measurements of summit emission rates where made on Crater Rim Drive in close proximity to a very active vent (Elias and Sutton, 2012) with SO_2 column densities routinely reaching values of $> 10^{19}$ molec cm^{-2} (Kern et al., 2012), it is perhaps not surprising that our emission rate estimates for 2008 to 2010 are comparably higher than the ground-based estimates.

However, in 2007 when summit emissions were negligible, our emission rates are actually lower than the ground-based values. During this time period, Elias and Sutton (2012) report significantly enhanced East Rift emissions coinciding with eruptive activity. The SO_2 emission rates from the East Rift were measured on Chain of Craters

ACPD
13, 28695–28727, 2013

Road, traversing beneath the plume at a distance of about 9 km from the Pu'u 'Ō'ō vent. At this point, the plume was significantly diluted, and the encountered column densities were much lower than those encountered at the summit vent. Therefore, non-linear absorption effects were probably negligible, especially before 2008 (Elias and Sutton, 2012).

In the absence of extremely high column densities, the ground-based SO_2 emission rates from the East Rift in 2007 are likely fairly accurate. For this time period, the discrepancy between satellite and ground-based emission rates instead appears to be caused by a change in the satellite AMF between 2007 and 2008: as mentioned before, the difference in altitude between the Kīlauea summit and East Rift emission plumes leads to a different sensitivity of the satellite instrument towards SO_2 emitted at each of the two locations. Prior to the opening of the Overlook Vent at Kīlauea's summit in 2008, the entire plume originated from the East Rift and was on average located at a lower altitude. Although it is difficult to accurately quantify the exact impact on the AMF without an accurate measurement of the plume altitude prior to 2008, it is clear that a lower plume would systematically reduce the sensitivity of the satellite towards SO_2, and this behavior is deemed the main cause for the discrepancy of satellite and ground-based results in 2007. In addition, the SO_2 lifetime might be shorter for the East Rift emissions (Porter et al., 2002), which would as well cause a low bias of emission rate estimates based on mean VCDs.

5 Conclusions

Satellite measurements provide new potential to investigate and quantify sources and transformations of atmospheric trace gases. By analysing the downwind plume of SO_2 from the Kīlauea volcano, SO_2 lifetimes and emission rates can be derived from GOME-2 observations and ECMWF wind fields, but without the need for a chemical model.

ACPD
13, 28695–28727, 2013

For the period of most active summit degassing in March–November 2008, we find monthly mean effective SO_2 lifetimes of 1–2 days, with highest lifetimes in summer, when cloud cover is small, and lowest in spring and autumn.

Emission rates in 2008 are estimated to 9–21 kt day^{-1}, which is significantly higher (about 3 times) than reported from ground based measurements. Further investigation is needed to explore this disagreement.

From the observed linear relation between emission rates and monthly mean column densities, emission rates can be roughly estimated also for months with lower SO_2 VCDs, where no clear downwind plume could be fitted. However, this approach only works as long as SO_2 lifetime and plume altitude do not change significantly.

An accurate a priori vertical trace gas and aerosol concentration profile is needed for the quantitative interpretation of SO_2 absorption measured by satellites. For an isolated "point source" (in terms of the satellite's spatial resolution) like Kīlauea, however, the plume altitude can be constrained from its downwind propagation direction (at least after the opening of the Overlook Vent at the summit in 2008).

Kīlauea turned out to be particularly suited for our approach, as (a) it is a singular, remote source of SO_2, (b) the outflow patterns are clear and constrained due to the steady trade winds, and (c) clouds turned out to be not critical. A similar analysis may, in principle, be performed on other strong point sources of SO_2, like other degassing volcanoes or strong industrial sources, but will probably be more challenging due to higher cloud fractions, higher wind variability, or interfering SO_2 sources.

The MetOp satellite series will provide a continuous time series covering more than 2 decades. Future satellite instruments like TROPOMI (Veefkind et al., 2012) will provide better spatial coverage (once per day) and have smaller ground pixels, resulting in a higher fraction of cloud-free observations. In addition, the better spatial resolution could potentially reveal a possibly different plume chemistry, i.e. effective SO_2 lifetime, close to the source. Furthermore, the expected better detection limit might facilitate the investigation of weaker sources of SO_2.

ACPD
13, 28695–28727, 2013

Acknowledgements. We thank A. J. Sutton (USGS) for valuable comments on this manuscript. We acknowledge EUMETSAT for providing GOME-2 spectra, ECMWF for providing wind fields, and NASA for providing aerosol optical depth from MODIS Terra. Contour lines are derived from SRTM topographic data provided by the US Geological Survey (http://dds.cr.usgs.gov/srtm/version2_1/SRTM3). Oliver Woodford is acknowledged for providing the MATLAB routine `export_fig`, which significantly simplifies the processing of MATLAB figures.

The service charges for this open access publication have been covered by the Max Planck Society.

References

Beirle, S., Platt, U., Von Glasow, R., Wenig, M., and Wagner, T.: Estimate of nitrogen oxide emissions from shipping by satellite remote sensing, Geophys. Res. Lett., 31, L18102, doi:10.1029/2004GL020312, 2004. 28697

Beirle, S., Boersma, K. F., Platt, U., Lawrence, M. G., and Wagner, T.: Megacity emissions and lifetimes of nitrogen oxides probed from space, Science, 333, 1737–1739, doi:10.1126/science.1207824, 2011. 28697, 28702, 28706

Beirle, S., Hörmann, C., Penning de Vries, M., and Wagner, T.: Estimating the Lifetime of SO_2 and Aerosols from Space: a Case Study for the Kīlauea Volcano, in: Proceedings of the ESA conference "ATMOS – Advances in Atmospheric Science and Applications", 18–22 June 2012, SP-708 (CD-ROM), Bruges, Belgium, 2012. 28699, 28707

Burrows, J. P., Weber, M., Buchwitz, M., Rozanov, V. V., Ladstätter-Weißenmayer, A., Richter, A., DeBeek, R., Hoogen, R., Bramstedt, K., and Eichmann, K. U.: The Global Ozone Monitoring Experiment (GOME): mission concept and first scientific results, J. Atmos. Sci., 56, 151–174, 1999. 28697

Callies, J., Corpaccioli, E., Eisinger, M., Hahne, A., and Lefebvre, A.: GOME-2-MetOp's second-generation sensor for operational ozone monitoring, ESA Bull., 102, 28–36, available at: http://www.esa.int/esapub/bulletin/bullet102/Callies102.pdf (accessed: 20 March 2013), 2000. 28698

ACPD

13, 28695–28727, 2013

Cao, G., Giambelluca, T. W., Stevens, D., and Schroeder, T.: Inversion variability in the Hawaiian trade wind regime, J. Climate, 20, 1145–1160, 2007. 28700

Carn, S. A., Strow, L. L., De Souza-Machado, S., Edmonds, Y., and Hannon, S.: Quantifying tropospheric volcanic emissions with AIRS: the 2002 eruption of Mt. Etna (Italy), Geophys. Res. Lett., 32, L02301, doi:10.1029/2004GL021034, 2005. 28697

Carn, S. A., Krueger, A. J., Arellano, S., Krotkov, N. A., and Yang, K.: Daily monitoring of Ecuadorian volcanic degassing from space, J. Volcanol. Geotherm. Res., 176, 141–150, doi:10.1016/j.jvolgeores.2008.01.029, 2008. 28697

Deutschmann, T., Beirle, S., Frieß, U., Grzegorski, M., Kern, C., Kritten, L., Platt, U., Prados-Roman, C., Pukite, J., Wagner, T., Werner, B., and Pfeilsticker, K.: The Monte Carlo atmospheric radiative transfer model McArtim: introduction and validation of Jacobians and 3-D features, J. Quant. Spectrosc. Ra., 112, 1119–1137, doi:10.1016/j.jqsrt.2010.12.009, 2011. 28698

Eguchi, K., Uno, I., Yumimoto, K., Takemura, T., Nakajima, T. Y., Uematsu, M., and Liu, Z.: Modulation of cloud droplets and radiation over the North Pacific by sulfate aerosol erupted from Mount Kīlauea, Sci. Onl. Lett. Atmos., 7, 77–80, doi:10.2151/sola.2011-020, 2011. 28697, 28701, 28704

Elias, T. and Sutton, A. J.: Sulfur dioxide emission rates from Kīlauea Volcano, Hawai'i, 2007–2010, US Geological Survey Open-File Report 2012–1107, available at: http://pubs.usgs.gov/of/2012/1107/ (accessed: 26 June 2012), 25 pp., 2012. 28697, 28701, 28704, 28705, 28709, 28710, 28711, 28719, 28726

Galle, B., Oppenheimer, C., Geyer, A., McGonigle, A. J. S., Edmonds, M., and Horrocks, L.: A miniaturised ultraviolet spectrometer for remote sensing of SO_2 fluxes: a new tool for volcano surveillance, J. Volcanol. Geotherm. Res., 119, 241–254, 2002. 28697

Hörmann, C., Sihler, H., Bobrowski, N., Beirle, S., Penning de Vries, M., Platt, U., and Wagner, T.: Systematic investigation of bromine monoxide in volcanic plumes from space by using the GOME-2 instrument, Atmos. Chem. Phys., 13, 4749–4781, doi:10.5194/acp-13-4749-2013, 2013. 28698, 28710

Horton, K. A., Williams-Jones, G., Garbeil, H., Elias, T., Sutton, A. J., Mouginis-Mark, P., Porter, J. N., and Clegg, S.: Real-time measurement of volcanic SO_2 emissions: validation of a new UV correlation spectrometer (FLYSPEC), Bull. Volcanol., 68, 323–327, doi:10.1007/s00445-005-0014-9, 2006. 28709

ACPD
13, 28695–28727, 2013

Kern, C., Deutschmann, T., Werner, C., Sutton, A. J., Elias, T., and Kelly, P. J.: Improving the accuracy of SO_2 column densities and emission rates obtained from upward-looking UV-spectroscopic measurements of volcanic plumes by taking realistic radiative transfer into account, J. Geophys. Res., 117, D20302, doi:10.1029/2012JD017936, 2012. 28710

Khokhar, M. F., Frankenberg, C., Van Roozendael, M., Beirle, S., Kühl, S., Richter, A., Platt, U., and Wagner, T.: Satellite observations of atmospheric SO_2 from volcanic eruptions during the time-period of 1996–2002, Adv. Space Res., 36, 879–887, 2005. 28697

Krotkov, N. A., Schoeberl, M. R., Morris, G. A., Carn, S., and Yang, K.: Dispersion and lifetime of the SO_2 cloud from the August 2008 Kasatochi eruption, J. Geophys. Res.-Atmos., 115, D00L20, doi:10.1029/2010JD013984, 2010. 28697

Lee, C., Martin, R. V., Van Donkelaar, A., Lee, H., Dickerson, R. R., Hains, J. C., Krotkov, N., Richter, A., Vinnikov, K., and Schwab, J. J.: SO_2 emissions and lifetimes: estimates from inverse modeling using in situ and global, space-based (SCIAMACHY and OMI) observations, J. Geophys. Res.-Atmos., 116, D06304, doi:10.1029/2010JD014758, 2011. 28704

Lelieveld, J., Roelofs, G., Feichter, J., and Rodhe, H.: Terrestrial sources and distribution of atmospheric sulphur, Philos. T. Roy. Soc. B, 352, 149–157, 1997. 28704

Leue, C., Wenig, M., Wagner, T., Klimm, O., Platt, U., and Jähne, B.: Quantitative analysis of NO_x emissions from Global Ozone Monitoring Experiment satellite image sequences, J. Geophys. Res., 106, 5493–5505, 2001. 28697

Moffat, A. J. and Millan, M. M.: The applications of optical correlation techniques to the remote sensing of SO_2 plumes using sky light, Atmos. Environ., 5, 677–690, 1971. 28697

Monks, P. S. and Beirle, S.: Applications of satellite observations of tropospheric composition, in: The Remote Sensing of Tropospheric Composition from Space, Springer-Verlag, Berlin, Heidelberg, 365–449, 2011. 28697

Mori, T. and Burton, M.: The SO_2 camera: a simple, fast and cheap method for ground-based imaging of SO_2 in volcanic plumes, Geophys. Res. Lett., 33, L24804, doi:10.1029/2006GL027916, 2006. 28697

Platt, U. and Stutz, J.: Differential Optical Absorption Spectroscopy, Springer-Verlag, Berlin, Heidelberg, 2008. 28698

Porter, J. N., Horton, K. A., Mouginis-Mark, P. J., Lienert, B., Sharma, S. K., Lau, E., Sutton, A. J., Elias, T., and Oppenheimer, C.: Sun photometer and lidar measurements of the plume from the Hawai'i Kīlauea Volcano Pu'u 'Ō'ō vent: aerosol flux and SO_2 lifetime, Geophys. Res. Lett., 29, 30-1–30-4, doi:10.1029/2002GL014744, 2002. 28704, 28711

ACPD
13, 28695–28727, 2013

Veefkind, J. P., Aben, I., McMullan, K., Förster, H., de Vries, J., Otter, G., Claas, J., Eskes, H. J., de Haan, J. F., Kleipool, Q., van Weele, M., Hasekamp, O., Hoogeveen, R., Landgraf, J., Snel, R., Tol, P., Ingmann, P., Voors, R., Kruizinga, B., Vink, R., Visser, H., and Levelt, P. F.: TROPOMI on the ESA Sentinel-5 Precursor: a GMES mission for global observations of the atmospheric composition for climate, air quality and ozone layer applications, Remote Sens. Environ., 120, 70–83, doi:10.1016/j.rse.2011.09.027, 2012. 28712

Von Glasow, R., Bobrowski, N., and Kern, C.: The effects of volcanic eruptions on atmospheric chemistry, Chem. Geol., 263, 131–142, doi:10.1016/j.chemgeo.2008.08.020, 2009. 28696

Wang, P., Stammes, P., van der A, R., Pinardi, G., and van Roozendael, M.: FRESCO+: an improved O_2 A-band cloud retrieval algorithm for tropospheric trace gas retrievals, Atmos. Chem. Phys., 8, 6565–6576, doi:10.5194/acp-8-6565-2008, 2008. 28698

Yuan, T., Remer, L. A., and Yu, H.: Microphysical, macrophysical and radiative signatures of volcanic aerosols in trade wind cumulus observed by the A-Train, Atmos. Chem. Phys., 11, 7119–7132, doi:10.5194/acp-11-7119-2011, 2011. 28697

ACPD
13, 28695–28727, 2013

Table 1. Baseline and alternative a priori settings and their impact on emission rate and lifetime estimates for March–November 2008.

	a priori	Baseline	Alternatives	$\Delta E/E$	$\Delta\tau/\tau$
(a)	Cloud fraction threshold	0.2			
			0.1	−4 %	−11 %
			0.3	−2 %	7 %
(b)	Latitude range	10–25° N			
			15–20° N	2 %	−17 %
			5–30° N	−9 %	1 %
(c)	Time interval	[−20,100] h			
			[−10,70] h	2 %	−1 %
			[−30,130] h	4 %	−4 %
			[20,100] h	10 %	5 %
(d)	Background correction	upwind			
			B from fit	5 %	5 %
(e)	Plume altitude	1.5–2.5 km			
			1–2 km	29 %	−8 %
			2–3 km	−25 %	32 %

ACPD
13, 28695–28727, 2013

Table 2. Effect of temporal variations of E and τ. For details see text.

T	$\tau_{\mathrm{Fit}}/\overline{\tau}$	$k_{\mathrm{Fit}}/\overline{k}$	$E_{\mathrm{Fit}}/\overline{E}$
1 h	0.74	0.99	1.04
10 h	0.81	0.91	1.04
100 h	1.02	0.71	0.96

ACPD
13, 28695–28727, 2013

Table 3. Monthly mean emission rates (in kt day^{-1}) from GOME-2 compared to Elias and Sutton (2012) (ES12) for Junes 2007–2010.

Year	GOME-2 (from Fit)	GOME-2 (from VCD)	ES12 (total)	ES12 (rift)	ES12 (summit)
2007		0.7	1.3	1.1	0.2
2008	12.5	11.2	2.8	1.9	0.9
2009		6.4	2.2	1.4	0.9
2010		5.3	1.3	0.5	0.8

ACPD
13, 28695–28727, 2013

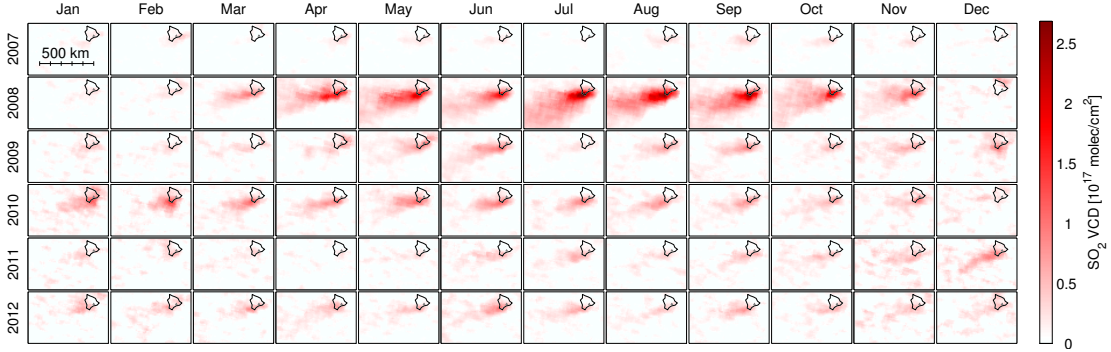

Fig. 1. Monthly mean SO_2 VCD 2007–2012. The upper end of the color scale corresponds to 10 DU. Each panel covers 161–154° W longitude and 16–20.5° N latitude (compare Fig. 2).

ACPD
13, 28695–28727, 2013

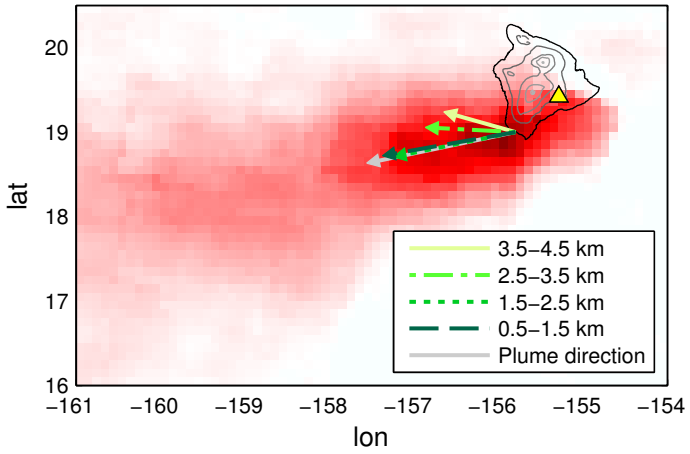

Fig. 2. Monthly mean SO_2 VCD for August 2008. Colorbar as in Fig. 1. Kīlauea on Hawai'i Island is indicated by a triangle. The grey lines show surface elevation contours in 1 km intervals. The main plume direction is indicated by a grey arrow, while the mean ECMWF wind vector for different altitudes is plotted in shades of green (a vector length of 1° corresponds to a velocity of 5 m s^{-1}). As transport on Hawai'i Island is strongly affected by topography, the south-western tip of the island was chosen as origin.

ACPD
13, 28695–28727, 2013

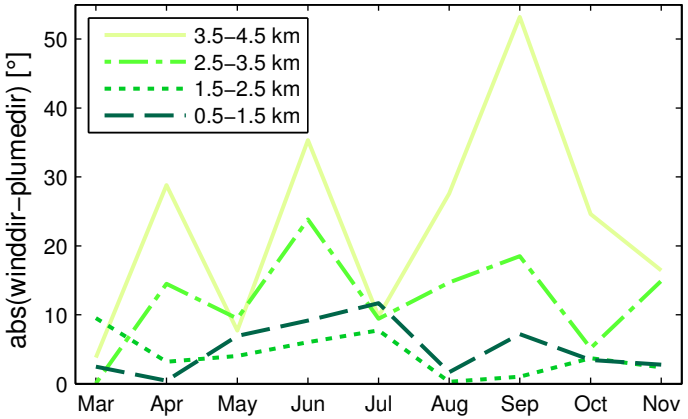

Fig. 3. Absolute deviation between the outflow direction of the SO_2 plume and the mean ECMWF wind direction for different altitudes for March–November 2008. Wind directions above 2.5 km do not match the observed movement of the plume.

ACPD
13, 28695–28727, 2013

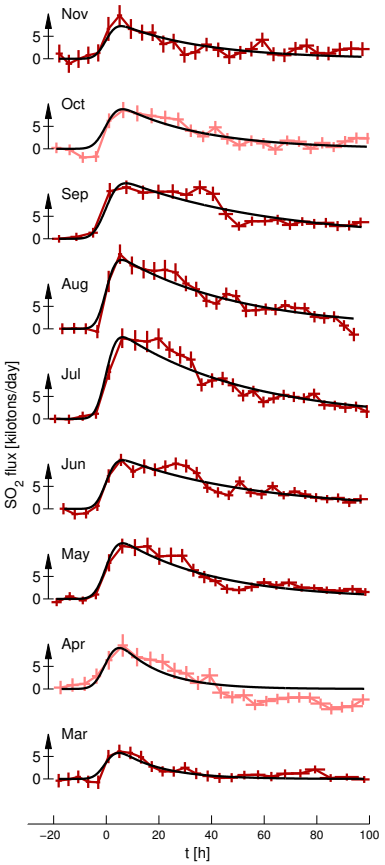

Fig. 4. Measured SO_2 flux (i.e., latitudinally integrated VCD times wind speed u) as function of time for March–November 2008 (red) and the fitted exponential downwind decay according to Eq. (1) (black). Light red indicates months in which ECMWF winds turned westerly for at least one 6 h time-step. Error bars in x and y reflect the statistical error of the mean SO_2 flux, and the statistical error of t deduced from ECMWF wind variability, respectively.

ACPD
13, 28695–28727, 2013

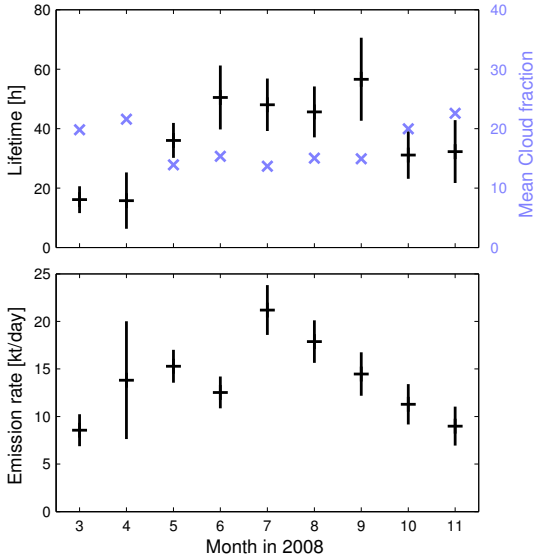

Fig. 5. Fitted SO_2 lifetimes (top) and emission rates (bottom) for March–November 2008. Error bars indicate the confidence intervals derived from the least-squares fit. In the upper panel, also the monthly mean cloud fraction (from GOME-2) is included, revealing an anti-correlation to τ ($R = -0.76$).

ACPD
13, 28695–28727, 2013

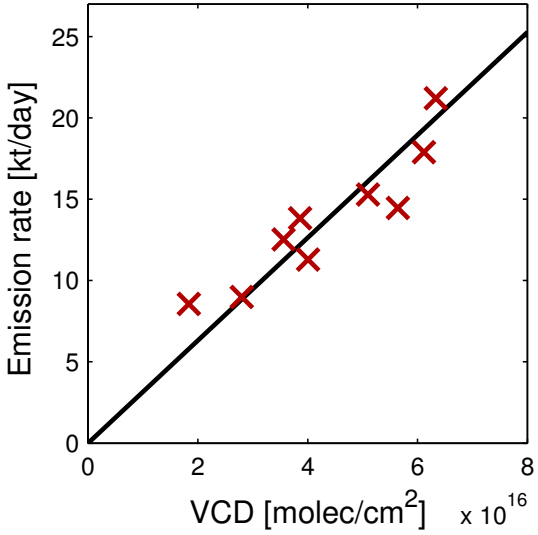

Fig. 6. Fitted monthly mean SO_2 emission rates vs. the respective mean SO_2 VCD (averaged over 17–20° N, 155–160° W) for March–November 2008. The correlation coefficient is $R = 0.92$. The black line represents a linear fit forced through origin.

ACPD
13, 28695–28727, 2013

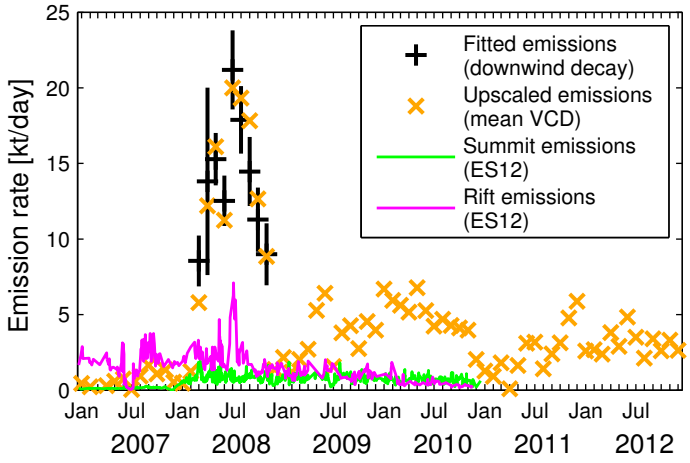

Fig. 7. Time series of Kīlauea's SO_2 emission rate. Black: results from the monthly fits (as in Fig. 5). Orange: emission estimates based on the monthly mean SO_2 VCD, using the linear relation derived in Fig. 6. Green/magenta: emission estimates by Elias and Sutton (2012) (ES12), derived from ground-based measurements, for the Kīlauea summit/East Rift, respectively.

ACPD
13, 28695–28727, 2013

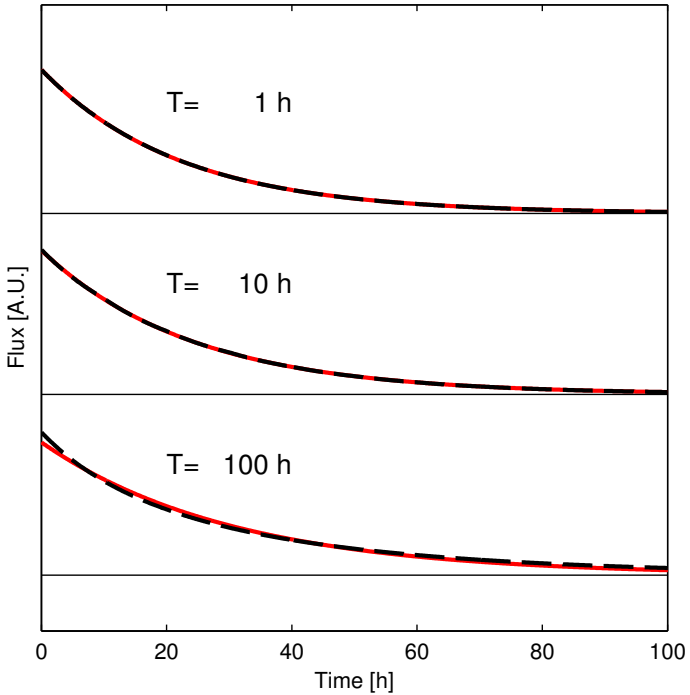

Fig. 8. Simulated (red, mean of 10 000 simulations) and fitted (black) downwind decay for varying input emission rates and instantaneous lifetimes, for different time intervals T over which the instantaneous lifetime is kept constant.

ACPD
13, 28695–28727, 2013